

BLADE INSTABILITY OF HORIZONTALLY STOPPABLE ROTORS

U. Arnold

Technical University of Braunschweig, Germany
 Institute of Flight Mechanics

Abstract

This paper investigates one important source for instability of stopped rotors during the decelerating and accelerating process. Flapping stability is usually lost at advance ratios above two, due to strong parameter excitation through periodic aerodynamic forces. Reducing the angular velocity of a hingeless rotor, on the other hand, increases the nondimensional flapping natural frequency that has a stabilizing effect. The differential equation of motion is set up for the common rigid blade approximation, considering spring restrained hinges with arbitrary hinge offset. Reverse flow, which will be shown to be decisive for the stability boundaries, is included analytically in a straightforward way. The effect of the parameter excitation is discussed by means of MATHIEU- and HILL-type differential equations. Simple stability criteria derived from STRUTT's stability diagram will be compared with the computed eigenvalues using FLOQUET theory. The effect of the forcing function i.e. the amplitude amplification of the inhomogeneous equation will be shown to be even more important than stability. Simulation results are presented in order to discuss the possibility of suppressing divergent flap oscillations by applying high rotor deceleration and acceleration rates.

Notation

c_{β}	flapping spring constant
D_0^m	mechanical flap damping
m_{bl}	blade mass
Q_{inst}	max. installed engine torque
V	rotorcraft velocity
v_i	induced velocity
x	nondimensional blade coordinate, state variable

β	flap angle
γ	LOCK-number / 2
$\delta = (\alpha V - v_i) / (\Omega R)$	inflow ratio
δ_3	pitch-flap coupling
ϑ_0	blade pitch angle
ϑ_1	blade twist
$\lambda = \text{Re}(\lambda) + j\text{Im}(\lambda)$ $= -\delta + j\omega$	eigenvalue of flapping motion
$\mu = V / (\Omega R)$	advance ratio
ν	forcing frequency
ψ	blade azimuth angle
Ω	rotor rotational speed, frequency of parameter excitation
$\bar{\omega}_{nt} = \sqrt{(c_{\beta} / I_{\beta})} / \Omega_{nom}$	nonrotating flapping natural frequency nondimensionalized by nominal rotor speed

All variables and quantities not listed here can be found in table 2 or in the appendix.

Introduction

A lot of R&D effort has been made to increase the cruise speed of different VTOL aircraft. While in its common helicopter configuration the rotorcraft achieves an excellent hover and vertical flight performance, which is due to the low disk loading, its efficiency drops rapidly as soon as the airspeed exceeds values of approximately 200 kt. One well-known solution, the Tilt Rotor aircraft, hopefully will enter production in the near future.

One rarely investigated alternative is to slow down the rotor horizontally as soon as higher forward speed is achieved, so all the required lift can be provided by a fixed wing. The rotor blades can then be folded and stowed in order to minimize the parasitic drag and to avoid aeroelastic problems such as flutter or divergence. Few configurations have been worked out in detail.

Ref.[1] describes a small research aircraft with two horizontally stoppable and stowable rotors side-by-side. The two convertible engines can be switched from shaft power mode to fan-jet thrust mode. Some calculations have been performed, investigating stability and control aspects during the transition/conversion phase. Rotor forces and moments have been computed, but the calculations did not cover aeromechanical problems in detail. First experience had been gained during wind tunnel tests of an earlier configuration called Me 408.

Two concept alternatives, namely a single versus a tandem rotor configuration have been investigated at NASA Ames, ref.[4]. Several important problems associated with the start/stop procedure (e.g. high shaft moments and vibrations) are discussed in that publication. Aeromechanical aspects have been studied in more detail during a Lockheed research program, ref.[2], that included wind tunnel tests of the full-scale stowable rotor system CL 870 in the NASA Ames 40x80 ft wind tunnel. The rotor was designed for eventual flight tests on the XH-51A compound helicopter. In that paper, time histories of the calculated and measured blade loads are presented as well as shaft moments for the entire acceleration and deceleration phase. Flapwise bending moments are also measured for the completely stopped rotor. The equations of motion are solved by numerical simulation. Ref.[5] presents further wind tunnel tests, concerning the behaviour of totally stopped rotor blades at higher airspeed. Stall flutter instabilities have been discovered in the retreating blade region.

The application of the so-called jet-flap rotor to a stoppable and stowable rotor aircraft is proposed in ref.[6]. This rotor concept was also tested in the NASA Ames wind tunnel. Flapping stability was ensured through active control using azimuth depending feedback gains. Another concept proposes to stop the rotor and to convert it into a fixed wing as described in ref. [3]. This, however, requires a completely different rotor design. On the other hand, common-sized rotors must be folded and stowed, because just to stop the rotor does not improve the drag characteristic compared to an unloaded, but rotating rotor, as it is pointed out in refs.[4,6].

Although the flapping instability at high advance ratios is generally well understood, there are few systematic investigations of this problem in connection with the stoppable rotor. Most of the previous published investigations, which are concerned with the flapping stability in forward flight, leave off at advance ratios well below one, refs.[7,8].

Two main effects are responsible for the occurrence of divergent flapping: on the one hand, the unloaded rotor operates at increasing advance ratios (up to infinity), if the rotor angular velocity is reduced while forward speed is constant. This results in strong parameter excitation due to periodic aerodynamic forces. On the other hand, the nondimensional natural flapping frequency rises, too. While the centrifugal force vanishes, the blade root stiffness gains importance in suppressing instability. The natural frequency of the nonrotating blade, which is nondimensionalized by the nominal rotor speed is used to describe this characteristic. The effect of $\bar{\omega}_{nr}$ is explained in fig.1, where the flapping natural frequency is shown versus the rotor speed. For the proposed and investigated rotors, $\bar{\omega}_{nr}$ ranges from 0.4 to 0.8, refs.[1,2]. Yet, a reduction of these high values may become desirable in order to limit rotor shaft moments. The ratio between the periodic excitation and the stabilizing constant stiffness will be shown to be decisive for the flapping behaviour.

The aim of this paper is to gain physical insight into such parameter excited instability and to derive some basic criteria for a feasible rotor design. The investigation presented here is based on the following simplified stopping process:

- vertical take-off and acceleration to transition speed in helicopter mode
- shifting the whole lift from the rotor to the wing
- slowing down, folding and stowing the rotor at constant forward speed
- wingborne acceleration to cruise speed.

Restarting the rotor is performed inversely. Tab.1 presents proposed design parameters and those chosen for this investigation.

High transition speed is usually preferred in order to enable a wing design that aims at optimal cruise performance. This, however, requires the application of high lift devices during transition and induces stronger stability problems for the stopped rotor blades before they are folded.

	Data as proposed in refs.[1+6]	Data applied in this investigation
disk loading	480__760	600 N/m ²
rotor solidity	6.9__12.7	7.6 %
thrust coeff.	0.07__0.18	0.08
blade tip speed	190__270	250 m/sec
transition speed	60__80	50 m/sec

Table 1: Main data of proposed stoppable rotor aircraft (hovering in rotorcraft mode)

The relationship between rotor angular velocity and advance ratio during rotor deceleration, which emerges from the chosen data, is shown in fig.2. As we proceed in this paper, we must always bear in mind, that both effects, namely the rise of the advance ratio and the reduction of the rotor speed, are involved simultaneously. First, we will concentrate on the isolated flapping degree of freedom at constant rotor speed. These results are of interest, if we postulate that it must be possible to interrupt and reverse the start/stop procedure at any time, see ref.[6]. Moreover, this simplified problem can be treated analytically and serve as the reference case for the transient simulations.

Blade Model

Flapping Equation of Motion

The inhomogeneous flapping equation is set up for a rigid, spring restrained blade. Hinge offset and spring stiffness are adjusted to obtain the desired natural frequency variation over the rotor speed. The derivation of the moments acting on the flapping hinge is presented in the appendix. This leads to the well known equation

$$\ddot{\beta} + [\gamma D(\psi) + 2 D_0^m] \Omega \dot{\beta} + [\gamma K(\psi) + K_0^m] \Omega^2 \beta = [\gamma E(\psi) + E_0] \Omega^2 \quad (1)$$

where $D(\psi)$, $K(\psi)$ and $E(\psi)$ are periodic coefficients, which emerge from the aerodynamic operating condition and therefore are strongly dependant on the advance ratio μ . The term K_0^m , which summarizes the spring effect of the centrifugal forces as well as the blade root restraint, depends on the rotor angular velocity. Additional mechanical damping can be incorporated by the constant D_0^m . Pitch-flap coupling is considered as $\tan \delta_3$ within the coefficient $K(\psi)$. The excitation by the forcing function $E(\psi)$ on the right hand side is due to inflow, blade twist and pitch, whereas the constant part E_0 describes the blade weight (see appendix). The blade data used for most of the following calculations are listed in tab.2 and are denoted as reference data.

ρ	1.225	kg/m ³	air density
g	9.81	m/sec ²	gravity constant
R	5.00	m	rotor radius
Ω_{nom}	50	rad/sec	nominal rotor speed
a/R	0.13		nondimensional hinge offset
\bar{m}	7.5	kg/m	blade mass per unit length (uniform mass distribution)
l_{Bl}	0.30	m	blade chord
$c_{a\alpha}$	6.25		lift curve slope
A	0.25		nondimensional aerodynamic blade origin
B	1.00		nondimensional aerodynamic blade end (tip loss factor)

Table 2: Reference data

So far, reverse flow has been neglected. This means, that the calculated lift acts in the wrong direction, as long as the retreating blade is crossing the reversed flow region. During the advance ratio increases, this region spreads out over all the azimuth range from π to 2π . The impact of this crude approximation is illustrated in fig.3. It should be noted, that the aerodynamic flapping damping $D(\psi)$ becomes negative for the retreating blade; an effect, which is physically impossible in this connection.

Various publications, e.g. refs.[7,9], mention that problem. Nevertheless, it seems to be useful to study the flapping behaviour, neglecting reverse flow. In this case, equation (1) can easily be splitted into two MATHIEU-Type differential equations, for which many comprehensive investigations have been conducted (see next chapter).

Consideration of Reverse Flow

If we assume an equal lift curve slope for flow from the leading edge or from the trailing edge respectively, then to change the sign of the lift coefficient in the corresponding region is a simple means of modelling reverse flow. In this case, the integrals with respect to the blade radius coordinate include the sign-function, as many authors have pointed out. They conclude that integration has to be splitted into the range from 0 to $-\mu \sin \psi$ and $-\mu \sin \psi$ to B. Since these limits depend on ψ some authors stress that there is no expression to be found, which would cover the whole azimuth range, e.g. ref.[7].

However, the appendix shows a rearrangement of the integrands in a way that enables an analytical, closed integration over the whole radius. The resulting functions $D_n^R(\psi)$ are illustrated in fig.4 for $n=0,1,2$. The incorporation of the periodic terms into the flapping equation instead of the constants D_n , leads to extended expressions for the coefficients $D^R(\psi)$, $K^R(\psi)$ and $E^R(\psi)$, which are listed in the appendix, as well. Despite the difference in formulation, these functions are equivalent to those published in ref.[7].

Flapping Stability of Slowed Rotor at Constant Rotor Speed

Most of the published investigations concerning the flapping stability cover the advance ratio range from hovering to about 0.5. As some authors propose (e.g. ref.[8]), a constant coefficient approximation based on the time averaged coefficients can be applied with reasonable accuracy. Fig.5 illustrates, however, what happens if this method is extended to stopped rotor problems. We know that the flapping motion is

sufficiently damped in hover. Increasing the advance ratio (while rotor speed is reduced) does not affect the nondimensionalized eigenvalue of an articulated rotor, whereas the flapping frequency (divided by the actual rotor speed) rises for a stiff rotor. Introducing the reverse flow model into the time average expressions, which of course is quite unrealistic, gives us a rough idea of the stabilizing effect of reverse flow. Yet, it has to be emphasized that no regions of instability occur in either case, in contrast to what we would expect to be a particular characteristic of a parameter excited system.

MATHIEU-Type Equation and STRUTT's Stability diagram

In order to become more familiar with the unusual behaviour of periodic systems, the well-known MATHIEU-Type differential equation will be discussed first. Since the flapping equation can be transformed into a very similar form, the same mathematical methods apply in order to examine stability. The homogeneous MATHIEU-Type equation is

$$\ddot{x} + 2D\Omega\dot{x} + (K_0 + K_C \cos \Omega t)\Omega^2 x = 0 \quad (2)$$

where the parameters D , K_0 and K_C represent the damping, the spring stiffness and the parameter excitation. Fig.6 above shows the STRUTT stability diagram that defines the stability boundaries in the K_0 - K_C parameter plane for $D=0$. This diagram has rarely been calculated for $K_C \gg 1$ (except e.g. ref.[13]). It can easily be extended to the case $D>0$, in which the unstable regions move back from the K_0 axis, as shown in refs.[13+16].

Let us assume that for a certain system, described by MATHIEU's equation, the parameters K_0 , K_C rise simultaneously, while D remains constant. This is illustrated in fig.6 for the trajectory $K_C=K_0$ and $D=0.15$. The two lower diagrams show the corresponding eigenvalues. In the regions of instability (for $D=0$), the real parts split in a way that one gains stability while the other loses it. This effect is called parameter resonance. But, since the trajectory always remains below the boundaries for $D=0.15$, stability is not lost.

As long as parameter resonance occurs, the eigenfrequency is engaged to an integral multiple of $\Omega/2$; that is to say it does not increase proportionally with the system stiffness $\sqrt{K_0}$. All stability diagrams presented in this paper have been calculated by the FLOQUET theory.

If we now remove the periodicity from the $D(\psi)$ term of the flapping equation (neglecting reverse flow) by the transformation

$$x = \beta e^{\frac{1}{2} \int_0^t (K_2 \gamma \mu \Omega \sin \Omega t) dt} \quad (3)$$

we get the HILL-type equation

$$\ddot{x} + 2D\Omega \dot{x} + (K_0 + K_C \cos \Omega t + K_{C2} \cos(2\Omega t + \varphi)) \Omega^2 x = 0 \quad (4)$$

Removing the whole damping term, along with its constant part, seems to be less useful, because in this case the stability behaviour of the transformed equation would not be directly comparable to that of equation (1).

The resulting parameters K_0 , K_C and K_{C2} , which depend on μ and Ω , are defined in the appendix. The constant damping is $D=K_1\gamma/2$. This extended MATHIEU-Type equation (4) is very similar to the one discussed above and has been studied in refs. [13,14,16] for phase angles of $\varphi=0$ and -180 deg. If K_C and K_{C2} are of the same magnitude, the influence of the phase angle on the stability boundaries, however, has to be considered (e.g. $\varphi=-129$ deg. for the reference data).

If we neglect the interaction of the K_C , K_{C2} terms though, stability for the slowed rotor can be discussed by two separated STRUTT diagrams, see fig.7. Calculating the two trajectories $K_C=f(K_0)$ and $K_{C2}=f(K_0)$, as well as the corresponding dampings, makes it obvious, that only the 2Ω term may cause instability for higher μ . Since the K_{C2} trajectory is a straight line, stability can easily be determined with the help of STRUTT's diagram. As an example, the required flapping spring stiffness has been calculated for the reference data. According to this, stability should be assured for $\bar{\omega}_{nr} \geq 0.170$, which is

very close to the exact result $\bar{\omega}_{nr} \geq 0.171$ obtained by the FLOQUET theory for the complete system. If the precise stability boundaries of STRUTT's diagram are not available for the corresponding damping, it may be useful to apply one of the very simple sufficient conditions given in ref. [15]. The most appropriate seems to be

$$K_C \leq (K_0 - D^2) \tanh 2\pi D \quad (5)$$

leading to $\bar{\omega}_{nr} \geq 0.196$, a boundary, which is by far on the safe side.

Effect of Reverse Flow and Modified Blade Characteristics on Stability

As it has been explained in the previous chapter, stability behaviour of parameter excited systems can be described by stability boundaries in the K_0 - K_C plane. For the flapping motion, however, it makes more sense to use parameters, which are physically connected with the stop rotor problem, as $\bar{\omega}_{nr}$ and μ (or $1/\Omega$). In order to estimate the current damping, the real part of the less stable eigenvalue can be embodied into the diagram as the third dimension, see fig.8 above. It is to be seen, that rising the flap hinge stiffness will stabilize the flapping motion at high advance ratios.

As supposed above, the consideration of reverse flow does actually improve the computed stability. The behaviour during rotor deceleration does not change in principle, but, the whole 3D stability pattern rises to higher damping with increasing advance ratio, as illustrated in fig.8 below. This becomes even more obvious in fig.9, where both real parts are plotted for an intersection at $\bar{\omega}_{nr} = \text{const} = 0.135$.

If we project these stability patterns back to the $\bar{\omega}_{nr}$ - μ plane, we obtain the two diagrams, fig.10, which are directly analogous to STRUTT's diagram. The shapes of the $\text{Re}(\lambda)/\Omega=0$ curves show clearly, that less flapping stiffness is required to assure stability, if reverse flow is modeled ($\bar{\omega}_{nr}=0.100$ for the referenz data). An other representation, that may be more common, is chosen in fig.11. It shows the corresponding root locus plots for $\bar{\omega}_{nr}=0.135$.

The influence of different blade design parameters on stability has been studied by numerous calculations based on the FLOQUET theory. For each case the nondimensional modal damping is plotted versus the advance ratio ($\mu=10/\Omega$) in fig.12 . The main results are:

- The most effective means to stabilize flapping is to increase the flap hinge stiffness.
- As long as reverse flow is neglected, negative pitch-flap coupling does improve stability. If reverse flow is considered, however, this coupling becomes destabilizing, regardless of the sign of δ_3 (fig.12, 1st and 4th column).
- Additional mechanical damping D_0^m increases all real parts to exactly the same degree, but it does not affect the gradient with respect to the advance ratio (fig.12, 5th column).
- If the LOCK number is reduced (i.e. the ratio of inertial to aerodynamic forces increases), the range of the real part variation becomes smaller, yet again, there is no significant change of the gradient to be observed (fig.12, 6th column).
- Reducing the hinge offset (without changing the flapping mass, but adjusting mass per unit length) slightly improves stability. Although the amplitudes of both $D(\psi)$ and $K(\psi)$ rise, the stabilizing effect of the increased positive $D(\psi)$ average predominates (fig.12, last column).

It has to be stressed that $\bar{\omega}_{nr}$ was held constant, where c_β was adjusted according to the flap inertia I_β . Moreover, it should be noted that calculations must be continued to advance ratios of at least 20, to enable the determination of a clear stability tendency.

Effect of Model Refinements

Since we are using such a straightforward model, we also have to discuss whether all applied simplifications are reasonable or not, regarding our problem. Therefore, the modal damping computed by two refined models has been compared to that by the standard model (for the reference case at the stability boundary). Fig.13 above presents the results obtained from a numerical, nonlinear blade model. It considers stall and compressibility (as well as reverse flow more precisely) utilizing 360 deg. profile data tables. Stability is evaluated from simulated time histories and shows excellent correlation.

When the rotor speed is reduced, the first flapwise mode shape changes considerably. One simple possibility is to schedule the hinge offset and stiffness for an optimal approximation of the mode shape (and the corresponding natural frequency) at each rotor speed. With this blade model, a slight unstable flapping behaviour has been computed, as shown in fig.13 below. That means, a proper representation of the changing mode shape should be incorporated in the model.

Forced Solution of Inhomogeneous Equation

During many investigations concerning compound rotorcraft design, the dynamic response turned out to be an important problem. Mainly, the impact of gusts on the flapping motion was studied, where pitch-flap coupling has often been proposed as an effective means to restrict flapping response. It will be shown that the response characteristic is also decisive for the stop rotor design.

In our case, the forcing function contains only integral multiples of Ω , as long as the blade pitch is held constant. But arbitrary discrete frequencies may occur on the right hand side, if specific control inputs are applied. Therefore it will firstly be discussed, which effect different forcing functions exhibit on the forced solution of parameter excited systems. Comprehensive surveys are given in refs.{13,14}.

Amplitude Curves of MATHIEU-Type Equation

Fig.14 summarizes the characteristics of the forced solution, again choosing the MATHIEU equation (2) as a simple example. The diagrams show the low FOURIER coefficients C_m of the forced solution

$$x_{\text{forced}} = \sum_{m=0}^{\infty} (C_m \cos(m\Omega t + \varphi_m)) \quad (6)$$

divided by the applied excitation amplitudes a_k of the forcing function

$$\dots = \Omega^2 \sum_{k=0}^{\infty} (a_k \cos k\Omega t) \quad (7)$$

plotted versus the system stiffness $K_O = (\omega_O/\Omega)^2$. From this, the following characteristics can be deduced:

- Even a constant term on the right hand side, as a_0 , produces a periodic response that contains all harmonics of Ω (incl. the 0th harm.). Peaks of the amplitude curves arise in the regions of the (n)-parameter resonances (fig.14 above).
- Forcing functions containing frequencies of $\nu = (m+1/2)\Omega$ lead to peaks in the regions of the (n+1/2)-parameter resonances (fig.14 2nd diagram).
- Analogous behaviour is observed for forcing frequencies of $\nu = m\Omega$ at all (n)-parameter resonances (fig.14 3rd diagram).
- For all other forcing frequencies, resonance peaks develop too, that is, whenever the system stiffness results in a real part of $\omega = n\Omega \pm \nu$ (fig.14 below).
- Those amplitude peaks turn out to be most critical, they are due to low forcing frequencies $m\Omega/2$ in the regions of the low parameter resonances. In the presented example, amplification gets to over 30, which is about 10 times stronger than it would be for a corresponding constant coefficient system.

Amplitude Curves of Flapping Equation

The following diagrams fig.15,16 present amplitude curves derived from the inhomogeneous flapping equation. The first six harmonics (0th to 5th) of the forced solution, related to the different parameters of the forcing function, are plotted versus the advance ratio. The constant term E_0 describes the effect of gravity. The influence of cyclic control inputs is represented by ϑ_0 , which determines the blade pitch variation $\Delta\vartheta = \vartheta_0 \cos\Omega t$ within the ϑ -term.

First of all, reverse flow is neglected again. It is seen that for the lowest stiffness of $\bar{\omega}_{nr} = 0.200$ all FOURIER coefficients increase to infinity (fig.15 left hand), whereas for $\bar{\omega}_{nr} = 0.220$ they remain limited, but at a very high level (fig.15 middle) and from just about $\bar{\omega}_{nr} = 0.240$ the amplitudes become reasonable (fig.15 right hand). It should be emphasized, that all cases are stable, since the corresponding stability boundary is already reached at $\bar{\omega}_{nr} = 0.170$ (compare fig.12a). As we expect, all amplitude peaks occur at those advance ratios, for which integral parameter-resonances are obtained (fig.15 bottom).

Modeling reverse flow, we get similar results, see fig.16. At the stability boundary $\bar{\omega}_{nr} = 0.100$ the amplitude rise proves to be very strong for all right hand side terms (fig.16 left hand). For $\bar{\omega}_{nr} = 0.145$ the amplitudes remain limited but again too high for any technical application (fig.16 middle). Only from a flap hinge stiffness of $\bar{\omega}_{nr} \geq 0.190$, rotor deceleration seems to be practicable (fig.16 right hand). Again, the relationship between amplitude curves and real parts of the homogeneous solution becomes obvious, but the individual amplitude peaks do not separate as sharply as in fig.14 and 15.

These calculations clearly establish the forced solution to be even more critical than the homogeneous problem (i.e.stability) with respect to the flapping motion of stop rotors.

Transient Flapping During Stop and Acceleration Process

So far, rotor speed has been assumed to be constant. Therefore, possible instabilities had an infinite period of time to develop fully. However, with respect to just flight mechanical aspects, the start/stop process has to be completed within a few seconds. The published investigations propose time intervals between 4 and 22 seconds. With the presented compound aircraft design, it takes a constant shaft torque of e.g. $72\%Q_{inst}$ within 3 sec. or $12\%Q_{inst}$ within 30 sec. to accelerate the rotor to nominal rotor speed. Since the small aerodynamic drag forces of an unloaded rotor are not sufficient to slow down the rotor in a definite time, a rotor brake must be used. Applying brake torques corresponding to $-65\%Q_{inst}$ within 3 sec. or $-4\%Q_{inst}$ within 30 sec. would be necessary to stop the rotor.

In order to study the dynamic flapping behaviour during the start/stop process, many numerical simulations have been performed, which lead to the time histories of the transient flap angle, shown in figs.17,18. Similar investigations directed to a quite different application can be found in ref.[11]. The flapping motion during rotor engagement and disengagement on board a ship at high wind conditions is discussed there.

Within the interesting μ region, rotor speed variation can be assumed to be linear with time achieving good accuracy. For the presented time histories rotor acceleration was set to $\dot{\Omega}=\pm 0.85\text{rad/sec}^2$ corresponding to a shaft torque of $\pm 3.5\%Q_{inst}$. As the results show, even such low rotor speed changes affect the flapping behavior considerably.

Fig.17 indicates that even for an articulated rotor ($\bar{\omega}_{nr}=0$) the flapping angle remains limited during the entire simulation. However, the inherent instability leads to unreasonably high amplitudes which are initiated either by a small initial disturbance applied to the homogeneous system (fig.17 3rd diagr.), or by the right hand side excitation (fig.17 4th and last diagr.). If the homogeneous system is stable for all μ (fig.18 3rd diagr.), only the forced solution exhibits to be critical. In the presented

example ($\bar{\omega}_{nr}=0.145$), the amplitude peaks have fallen to almost acceptable values (fig.18 4th and last diagr.).

Considering only the absolute maximum observed during each simulation, a great number of those calculations can be described by one single diagram as fig.19 or 20. First, the homogeneous solutions (excited by a $\Delta\delta$ step) have been evaluated for different Ω , fig.19. It becomes obvious that through the application of high shaft torque flap amplitudes can be restricted to feasible values even for quite instable cases. It is worthwhile mentioning that, due to the changing phase shift between initial disturbance and parameter excitation, the β_{max} values vary strongly between the plotted curves and very small values (destructive interference). Fig.20 shows a similar trend as above for the forced solutions. However, the positive influence of high Ω is somewhat smaller.

Hence it is seen, that to shorten the start/stop procedure by providing high torque to the rotor shaft is a possible means to augment flapping stability. However, it does not seem to be appropriate to base the rotor design on this fact, as possible clutch or brake failures etc. must be taken into account.

Conclusions and Outlook

Flapping stability behaviour of stopped rotors can easily be explained regarding the MATHIEU-type equation and STRUTT's stability diagram. As we expected, modelling reverse flow exhibits a considerable influence on calculated damping. A most compact analytical formulation is proposed as a direct extension of the case without reverse flow. The typical characteristics of parameter excited systems can be identified clearly in both cases.

During the investigation the flap hinge stiffness expressed by $\bar{\omega}_{nr}$ proved to be the decisive parameter:

- Flapping stability is achieved at about $\bar{\omega}_{nr}=0.1$
- Flapping amplitudes remain limited from about $\bar{\omega}_{nr}=0.2$

- Rotors proposed, investigated or tested by other authors are designed for $\bar{\omega}_{nr} = 0.4 + 0.8$

With respect to only the flapping behaviour, the latter values seem to be quite high, since they lead to undesired strong shaft moments. Numerical simulations show that the application of high rotor deceleration and acceleration rates is another means to reduce flapping amplitudes considerably.

The appropriate modeling of the changing flap mode shape turned out to be important. At least hinge offset scheduling will be regularly used within future calculations. In the reverse flow region the aerodynamic forces act approximately at 75% chord far away from the feathering axis and the center of gravity. Obviously, feathering moments are induced, which excite the torsional blade motion. In ref.[9] it has been shown that this effect can diminish flapping stability. Therefore, the torsional degree of freedom will be incorporated as a further step towards model refinement.

Lead-lag motion is expected to have small influence on the results, since the unloaded rotor (with $\vartheta_0 = 0, \beta_0 = 0$) develops only slide couplings between flap and lag motion. However, in the region of frequency cross-over, stability should be examined.

Many authors point out that the influence of unsteady aerodynamics, commonly modeled as dynamic inflow, decreases with rising advance ratio. But when the rotor speed is reduced to very low values, other aerodynamic effects gain importance e.g. radial flow. Moreover, unusual stability problems may occur as fixed wing divergence or flutter (see ref.[5]).

One important question has been fully neglected here: how to control the rotor during the start/stop procedure? Deloading must be assured within a certain angle of attack range, while shaft moments are narrowly restricted with respect to flight mechanical demands. These problems lead directly to the application of active control techniques. One possible approach is proposed in ref.[10], where flapping stabilization through cyclic pitch feedback control has been investigated. But as the decelerating

blades increasingly undergo different external disturbances and, due to this fact, the rotor loses tracking, concepts like the Individual Blade Control seem to be more appropriate in this case.

Appendix

The index 'R' indicates that reverse flow is modeled by switching the sign of the aerodynamic moment in the reverse flow region. If the index is omitted, reverse flow is either neglected or the formulation is identical for both cases.

Derivation of flapping equation of motion

Flow conditions at blade section:

- tangential velocity $v_t = \Omega R [x + \mu \sin \psi]$

- normal velocity

$$v_n = \Omega R \left[\delta - \frac{\dot{\beta}}{\Omega} \left(x - \frac{a}{R} \right) - \mu \beta \cos \psi \right]$$

Blade angles:

- blade pitch $\vartheta = \vartheta(\psi) + \vartheta_1 x - \beta \tan \delta_3$

- angle of attack

$$\alpha_{eff} = \left(\frac{v_n}{v_t} + \vartheta \right) \quad \alpha_{eff}^R = \left(\frac{v_n + \vartheta v_t}{|v_t|} \right)$$

Moments acting about the flap hinge:

- inertial moment $M_B^{inert} = -I_B \ddot{\beta}$

- aerodynamical moment $M_B^{aero} = \frac{\rho}{2} |c_{aw} R|^2 \int_A^B \alpha_{eff}^2 v_t^2 \left(x - \frac{a}{R} \right) dx$

- centrifugal moment $M_B^{centr} = -I_B^* \Omega^2 \beta$

- moment of hinge spring $M_B^{spring} = -c_B \beta$

- moment of gravity $M_B^g = -M_B^g \beta$

Definition of blade characteristics:

- LOCK number / 2 $\gamma = \frac{\rho / 2 c_{aw} |R|^4}{I_B}$

- flap moments of inertia

$$I_B = \int_{m_{b1}} (r-a)^2 dm \quad I_B^* = \int_{m_{b1}} r(r-a) dm$$

- flap mass moment

$$M_B^g = \int_{m_{b1}} (r-a) dm$$

Flapping equation:

$$\ddot{\beta} + \left[\gamma D(\psi) + 2 D_0^m \right] \Omega \dot{\beta} + \left[\gamma K(\psi) + K_0^m \right] \Omega^2 \beta = \left[\gamma E(\psi) + E_0 \right] \Omega^2$$

Coefficients:

- damping term

$$D(\psi) = K_1 + K_2 \mu \sin \psi$$

$$D^R(\psi) = K_1^R + 2 K_2^R \mu \sin \psi + K_3^R \mu^2 \sin^2 \psi$$

- spring term

$$K(\psi) = K_6 \mu \cos \psi + K_7 \mu^2 \cos \psi \sin \psi + (K_5 + 2 K_6 \mu \sin \psi + K_7 \mu^2 \sin^2 \psi) \tan \delta_3$$

$$K^R(\psi) = K_6^R \mu \cos \psi + 2 K_7^R \mu^2 \cos \psi \sin \psi + K_8^R \mu^3 \cos \psi \sin^2 \psi + (K_5^R + 3 K_6^R \mu \sin \psi + 3 K_7^R \mu^2 \sin^2 \psi + K_8^R \mu^3 \sin^3 \psi) \tan \delta_3$$

- forcing function

$$E(\psi) = (K_4 + 2 K_5 \mu \sin \psi + K_6 \mu^2 \sin^2 \psi) \vartheta_1 + (K_5 + 2 K_6 \mu \sin \psi + K_7 \mu^2 \sin^2 \psi) \vartheta(\psi) + (K_6 + 2 K_7 \mu \sin \psi) \delta$$

$$E^R(\psi) = (K_4^R + 3 K_5^R \mu \sin \psi + 3 K_6^R \mu^2 \sin^2 \psi + K_7^R \mu^3 \sin^3 \psi) \vartheta_1 + (K_5^R + 3 K_6^R \mu \sin \psi + 3 K_7^R \mu^2 \sin^2 \psi + K_8^R \mu^3 \sin^3 \psi) \vartheta(\psi) + (K_6^R + 2 K_7^R \mu \sin \psi + K_8^R \mu^2 \sin^2 \psi) \delta$$

- natural frequency (in hover)

$$K_0^m = \frac{I_B^* + c_B / \Omega^2}{I_B} = \left(\frac{\omega_{0B}}{\Omega} \right)^2_{\mu = \tan \delta_3 = 0}$$

- gravity term

$$E_0 = - \frac{M_B^* / \Omega^2}{I_B} g$$

Abbreviations:

$$K_4 = D_5 - \frac{a}{R} D_4$$

$$K_5 = D_4 - \frac{a}{R} D_3$$

$$K_1 = D_4 - 2 \frac{a}{R} D_3 + \left(\frac{a}{R} \right)^2 D_2$$

$$K_6 = D_3 - \frac{a}{R} D_2$$

$$K_2 = D_3 - 2 \frac{a}{R} D_2 + \left(\frac{a}{R} \right)^2 D_1$$

$$K_7 = D_2 - \frac{a}{R} D_1$$

$$K_3 = D_2 - 2 \frac{a}{R} D_1 + \left(\frac{a}{R} \right)^2 D_0$$

$$K_8 = D_1 - \frac{a}{R} D_0$$

Blade integrals:

$$D_n = \int_A^B x^{n-1} dx = \frac{1}{n} (B^n - A^n)$$

$$D_n^R = \int_A^B \frac{x^n}{|x + \mu \sin \psi|} dx = \frac{1}{n} (|B + W| B^{n-1} - |A + W| A^{n-1} - (2n-1) W D_{n-1}^R - (n-1) W^2 D_{n-2}^R)$$

$$\text{where } D_0^R = \ln \left| \frac{B+W}{A+W} \right| \quad \text{and} \quad W = \mu \sin \psi$$

MATHIEU-type equation

inhomogeneous equation with damping:

$$\ddot{x} + 2 D \Omega \dot{x} + (K_0 + K_C \cos \Omega t) \Omega^2 x = \Omega^2 \sum_{k=0}^{\infty} (a_k \cos k \Omega t)$$

homogeneous solution:

$$x_{\text{hom}} = p_1(t) e^{\lambda_1 t} + p_2(t) e^{\lambda_2 t} \quad \text{where} \quad p(t) = p(t + \frac{2\pi}{\Omega})$$

forced solution:

$$x_{\text{forced}} = \sum_{m=0}^{\infty} (C_m \cos(m \Omega t + \varphi_m))$$

Transformation of flapping equation to HILL-Type

Transformation:

$$x = \beta e^{\frac{1}{2} \int_0^t (K_2 \gamma \mu \Omega \sin \Omega t) dt}$$

HILL-Type equation:

$$\ddot{x} + 2 D \Omega \dot{x} + (K_0 + K_C \cos \Omega t + K_{C2} \cos(2 \Omega t + \phi)) \Omega^2 x = 0$$

Coefficients:

- constant term $K_0 = K_0^m - \frac{1}{8} K_2^2 \gamma^2 \mu^2$

- 1Ω excitation $K_C = \frac{1}{2} \gamma \mu \sqrt{(2K_6 - K_2)^2 + K_1^2 K_2^2 \gamma^2}$

- 2Ω excitation $K_{C2} = \frac{1}{2} \gamma \mu^2 \sqrt{K_7^2 + K_2^4 \gamma^2 / 16}$

- constant damping $D = \frac{1}{2} \gamma K_1$

References

- [1] H.Huber, H.Krafka, Studies on Rotor and Flight Dynamics of a Horizontally Stoppable Hingeless Rotor Aircraft, Forum Proceedings of the 2nd European Rotorcraft and Powered Lift Forum, Paper No.38, Sept.1976
- [2] R.E.Donham, W.P.Harvick, Analysis of Stowed Rotor Aeroelastic Characteristics, Journal of the American Helicopter Society, Vol.12, (1), Jan.1967
- [3] R.J.Huston, J.P.Shivers, The Conversion of the Rotor/Wing Aircraft, AGARD Conference Proceedings: Fluid Dynamics of Rotor and Fan Supported Aircraft at Subsonic Speeds, Göttingen, Sept.1967
- [4] W.H.Deckert, J.L.McCloud, Considerations of the Stopped Rotor V/STOL Concept, Journal of the American Helicopter Society, Vol.13, (1), Jan.1968
- [5] R.P.White, Jr., Instabilities Associated with a Rotor Blade Stopped in Flight, Journal of the American Helicopter Society, Vol.14, (2), Apr.1969
- [6] M.Kretz, Stoppable and Stowable Jet-Flap Rotor Concept, Forum Proceedings of the 4th European Rotorcraft and Powered Lift Aircraft Forum, Paper No.46, Sept.1978
- [7] G.J.Sissingh, Dynamics of Rotors Operating at High Advance Ratios, Journal of the American Helicopter Society, Vol.13, (3), July 1968
- [8] J.C.Biggers, Some Approximations to the Flapping Stability of Helicopter Rotors, Journal of the American Helicopter Society, Vol.19, (4), Oct.1974

- [9] G.J.Sissingh, W.A.Kuczynski, Investigations on the Effect of Blade Torsion on the Dynamics of the Flapping Motion, Journal of the American Helicopter Society, Vol.15, (2), Apr.1970
- [10] R.A.Calico, W.E.Wiesel, Stabilization of Helicopter Blade Flapping, Journal of the American Helicopter Society, Vol.31, (4), Oct.1986
- [11] S.J.Newman, A Theoretical Model for Predicting the Blade Sailing Behaviour of a Semi-Rigid Rotor Helicopter, Vertica, Vol. 14, (4), 1990
- [12] K.Klotter, G.Kotowski, Über die Stabilität der Lösungen Hillscher Differentialgleichungen mit drei unabhängigen Parametern, Zeitschrift für angewandte Mathematik und Mechanik, Band 23, (3), June 1943
- [13] G.Kotowski, Lösungen der inhomogenen Mathieuschen Differentialgleichung mit periodischer Störfunktion beliebiger Frequenz, Zeitschrift für angewandte Mathematik und Mechanik, Band 23, (4), Aug.1943
- [14] N.Eicher, Einführung in die Berechnung parametererregter Schwingungen, Dokumentation Weiterbildung der Technischen Universität Berlin, Heft 1, 1981
- [15] J.A.Richards, Analysis of Periodically Time-Varying Systems, Communications and Control Engineering Series, Springer-Verlag Berlin Heidelberg New York, 1983
- [16] N.Eicher, Ein Iterationsverfahren zur Berechnung des Stabilitätsverhaltens Zeitvarianter Systeme, VDI Fortschritt-Berichte, Reihe 11, Nr.63, 1984

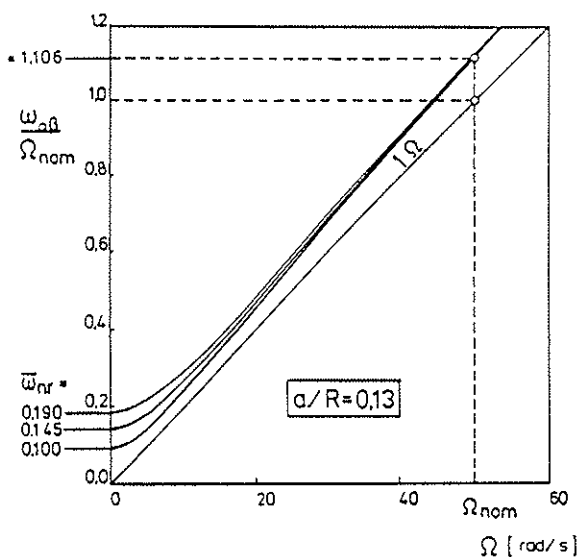


Figure 1: Effect of flapping stiffness $\bar{\omega}_{fl} = \omega_{fl}(\Omega=0)/\Omega_{nom}$ on flapping natural frequency versus rotor speed

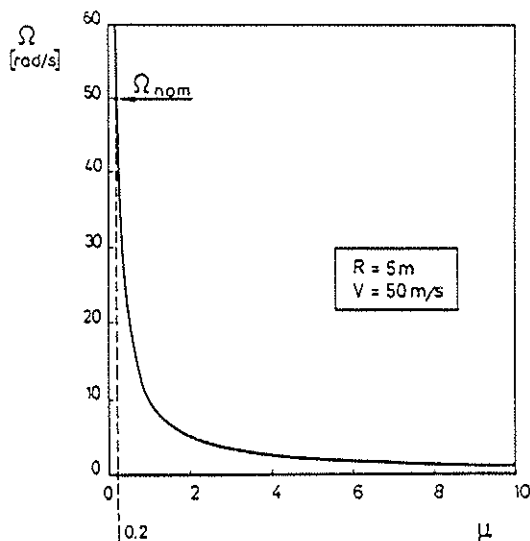


Figure 2: Rotor speed versus advance ratio at constant forward speed

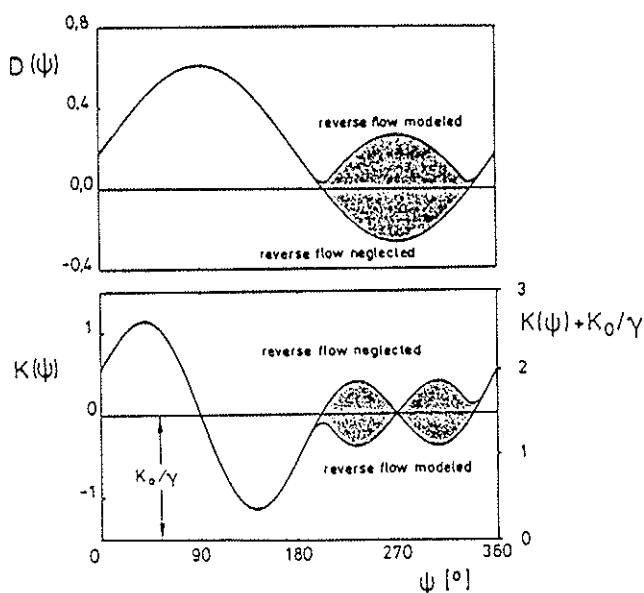


Figure 3: Effect of neglecting reverse flow on the coefficients of the flapping equation ($\mu=2, 10\% \Omega_{nom}, \bar{\omega}_{nr}=0.2$)

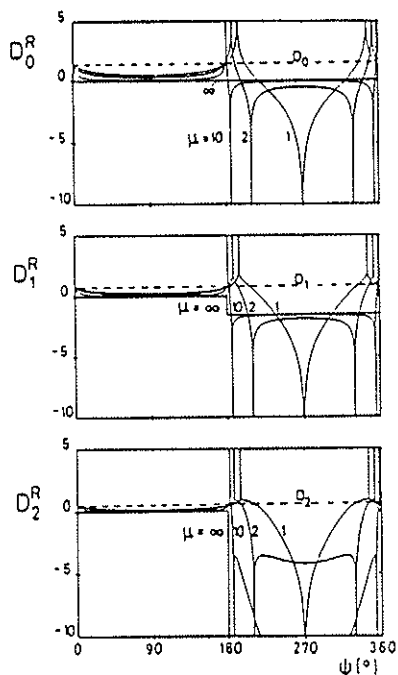


Figure 4: Redefined blade integrals considering reverse flow

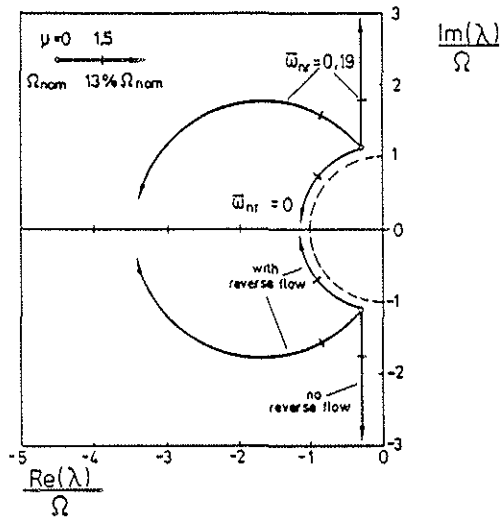


Figure 5: Root loci of flapping motion during rotor decelerating applying the constant coefficient approximation

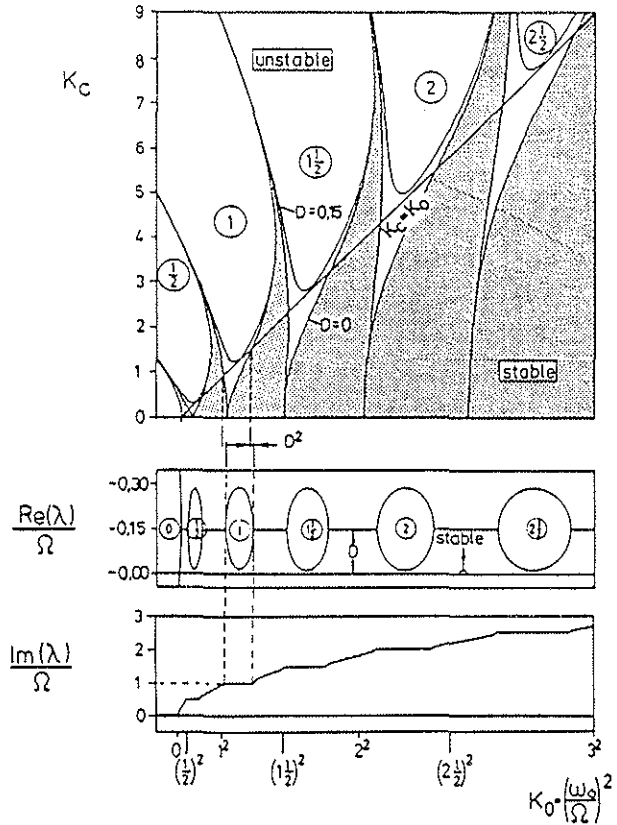


Figure 6: STRUTT's stability diagram and solution of the homogeneous damped MATHIEU-type equation for $K_C=K_0$

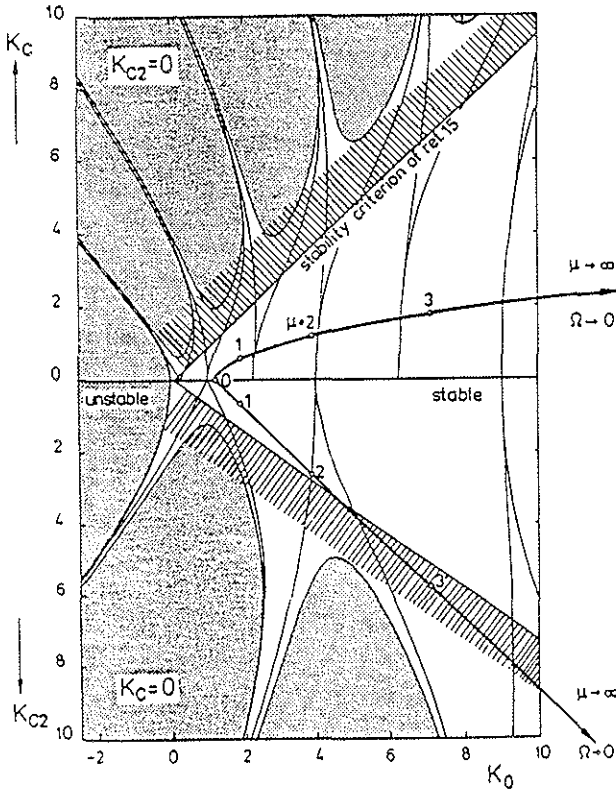


Figure 7: Stability of flapping equation (transformed to HILL-Type) emerging from STRUTT's stability diagram during rotor deceleration ($\omega_{nr}=0.17$, reverse flow neglected)

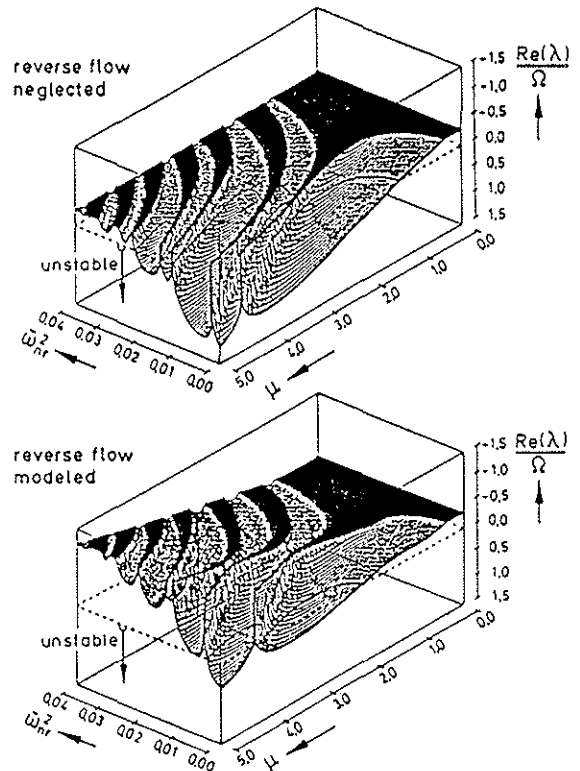


Figure 8: Effect of advance ratio and flap spring rate on flapping stability

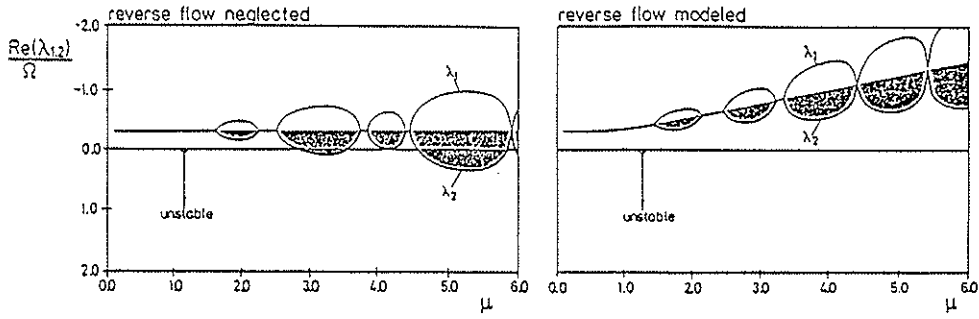


Figure 9: Effect of reverse flow on eigenvalues of flapping motion versus advance ratio ($\mu=10/\Omega$, $\bar{\omega}_{nr}=0.135$)

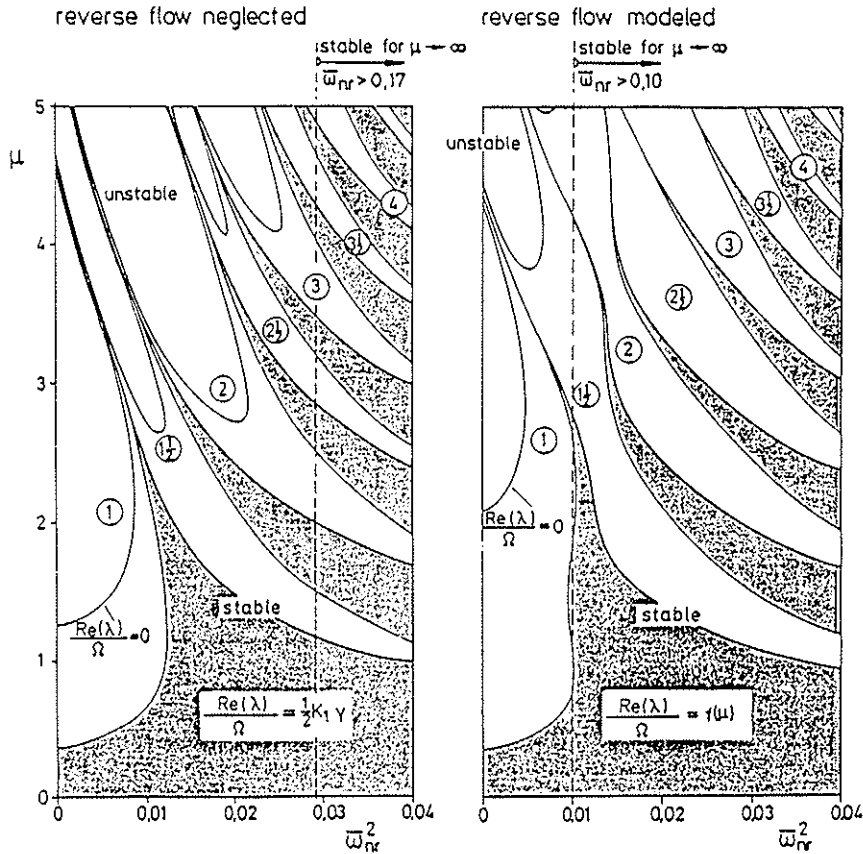


Figure 10: Stability diagrams of flapping motion (analogous to STRUTT'S diagram for MATHIEU equation)

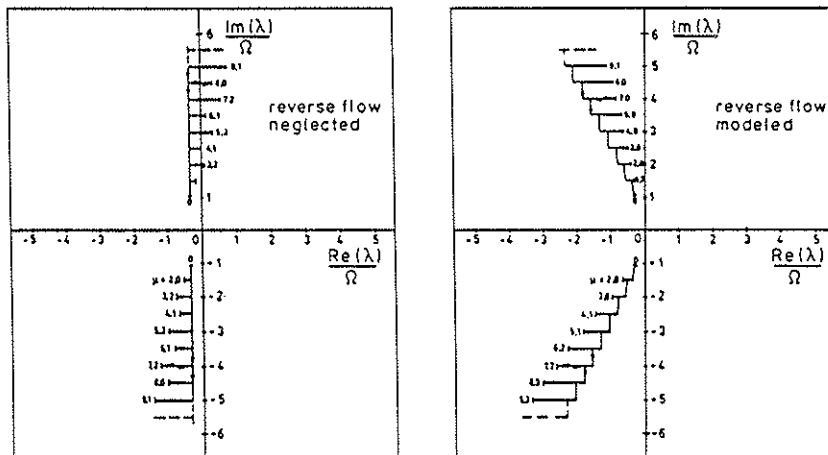


Figure 11: Effect of flapping spring rate and reverse flow on root loci of flapping motion at high advance ratios ($\bar{\omega}_{nr}=0.135$)

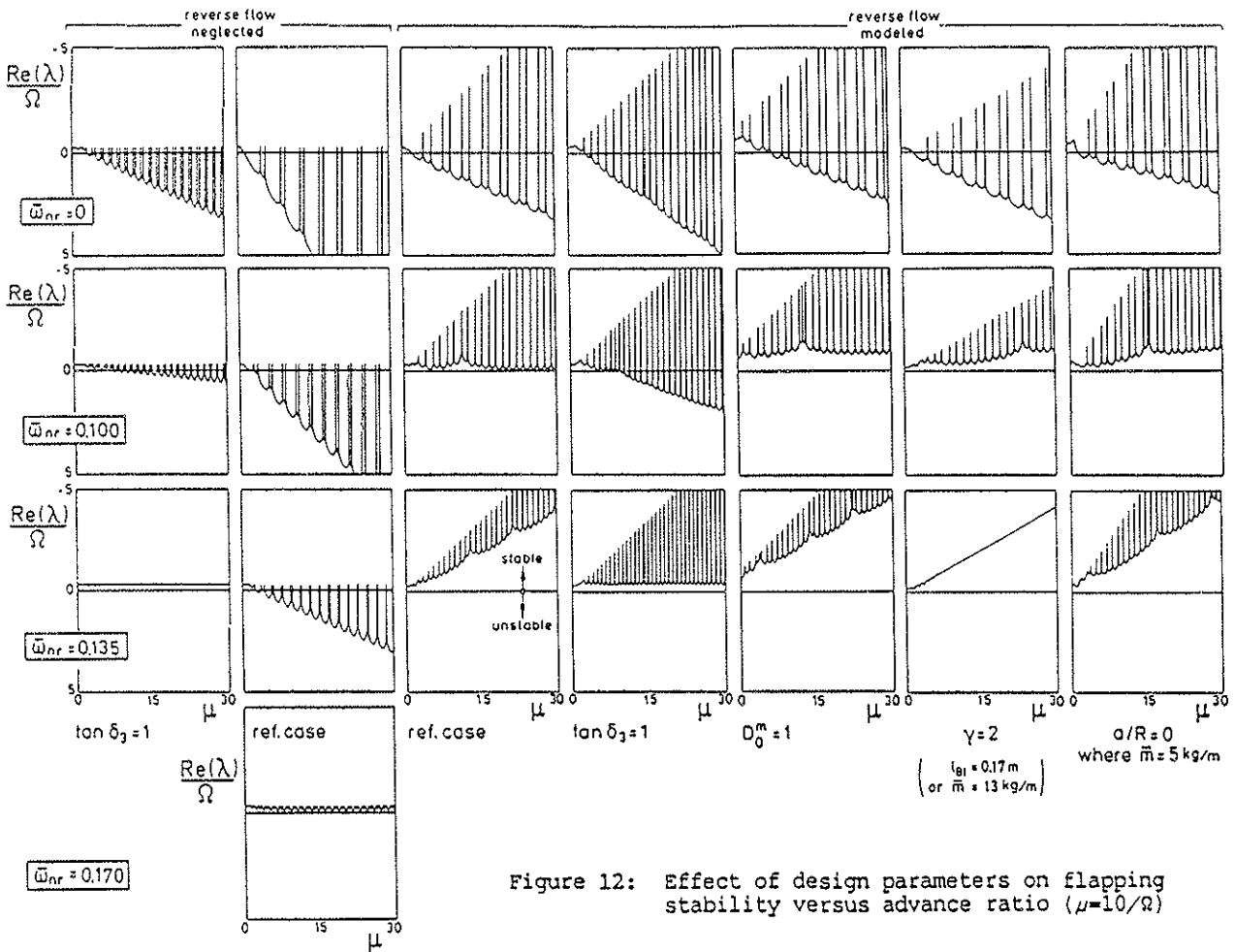
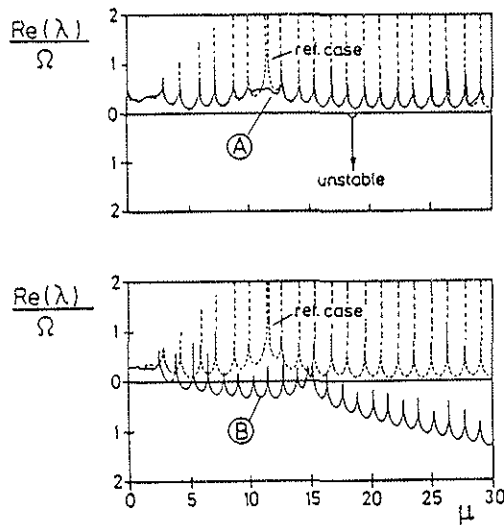


Figure 12: Effect of design parameters on flapping stability versus advance ratio ($\mu=10/\Omega$)



	mechanical model	aerodynamical model	flapping equation	stability analysis
ref. case	rigid blade, constant equiv. hinge offset and spring stiffness	linear, reverse flow modeled	linear	FLOQUET Theory
A	see ref. case	nonlinear, 360° profile data including reverse flow and stall	nonlinear	evaluation of num. integrated transient time histories
B	rigid blade, scheduled hinge offset and spring stiffness for best mode shape approx.	see ref. case	see ref. case	see ref. case

Figure 13: Effect of two different model refinements ($\bar{\omega}_{nr} = 0.100$)

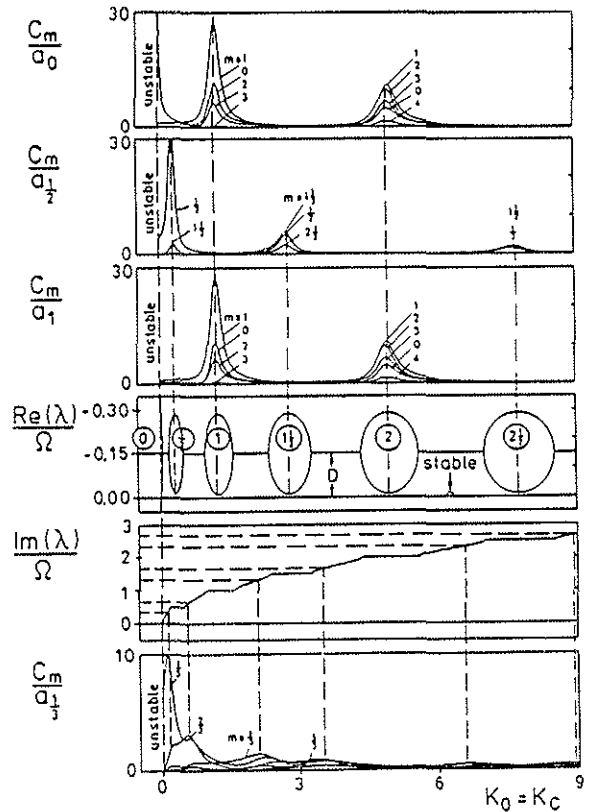


Figure 14: Amplitude curves of forced solution of MATHIEU equation for different forcing frequencies

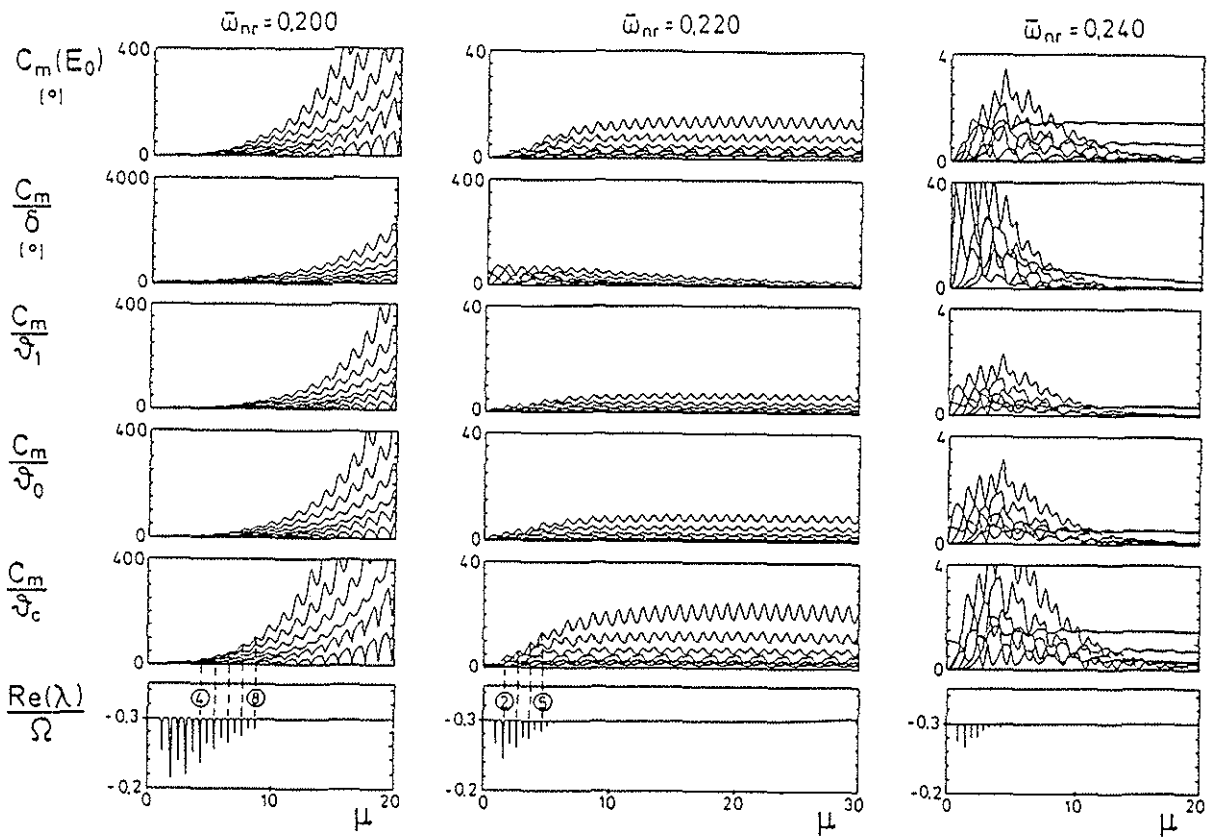


Figure 15: Amplitude curves for forced solution of inhomogeneous flapping equation versus advance ratio ($\mu=10/\Omega$). Effect of different forcing function terms and flap stiffness on the first five harmonics (reverse flow neglected)

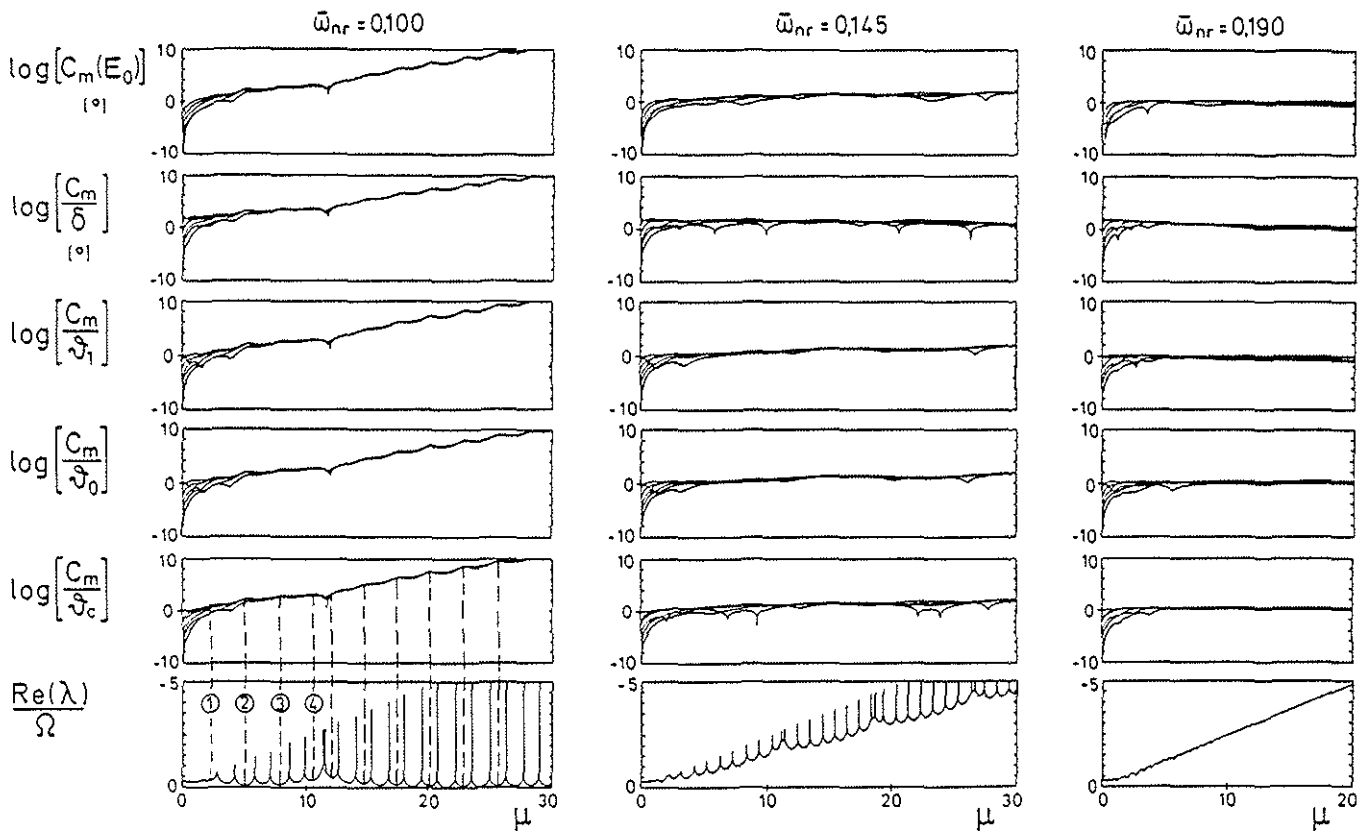


Figure 16: Amplitude curves for forced solution of inhomogeneous flapping equation versus advance ratio ($\mu=10/\Omega$). Effect of different forcing function terms and flap stiffness on the first five harmonics (reverse flow modeled)

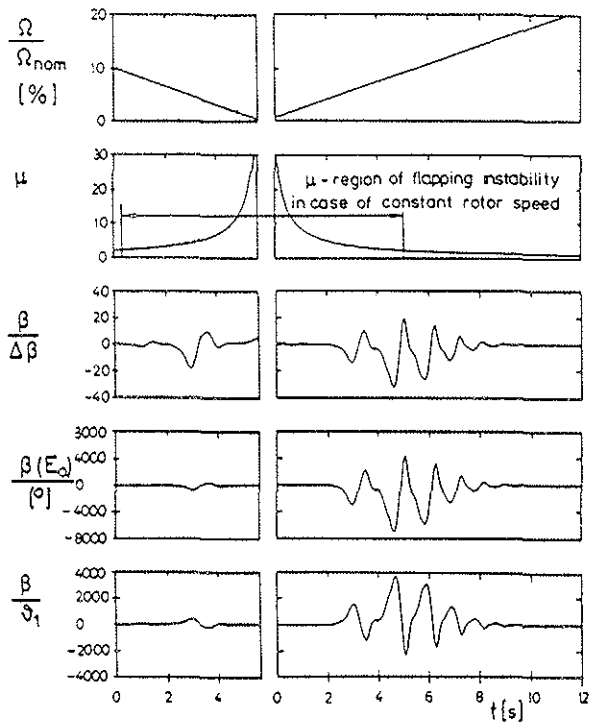


Figure 17: Flapping time histories of stop/restart procedure for articulated blade with $\Delta\beta$ as excitation of homogeneous equation and E_0, ϑ_1 -terms as forcing function of the inhomogeneous equation ($\bar{\omega}_{nr}=0, \Omega=const.=\pm 0.85\text{rad/sec}^2$)

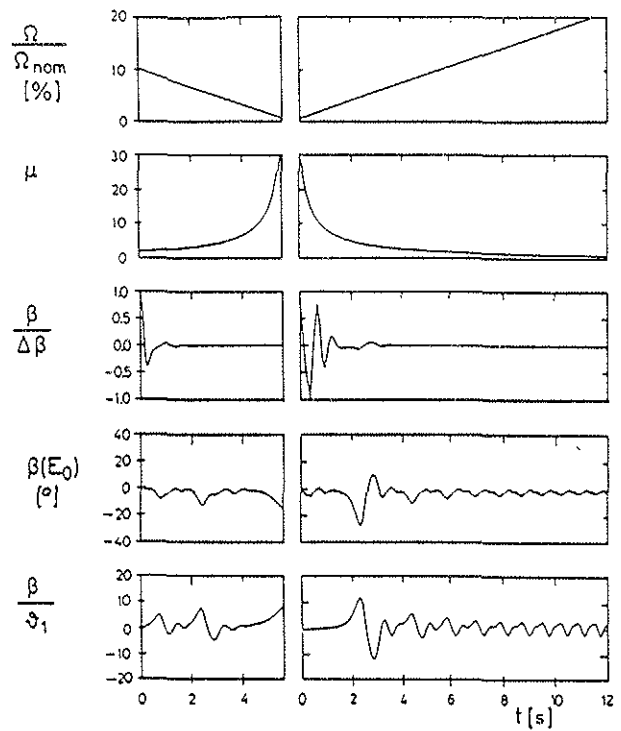


Figure 18: Flapping time histories of stop/restart procedure for rigid blade with $\Delta\beta$ as excitation of homogeneous equation and E_0, ϑ_1 -terms as forcing function of the inhomogeneous equation ($\bar{\omega}_{nr}=0.145, \Omega=const.=\pm 0.85\text{rad/sec}^2$)

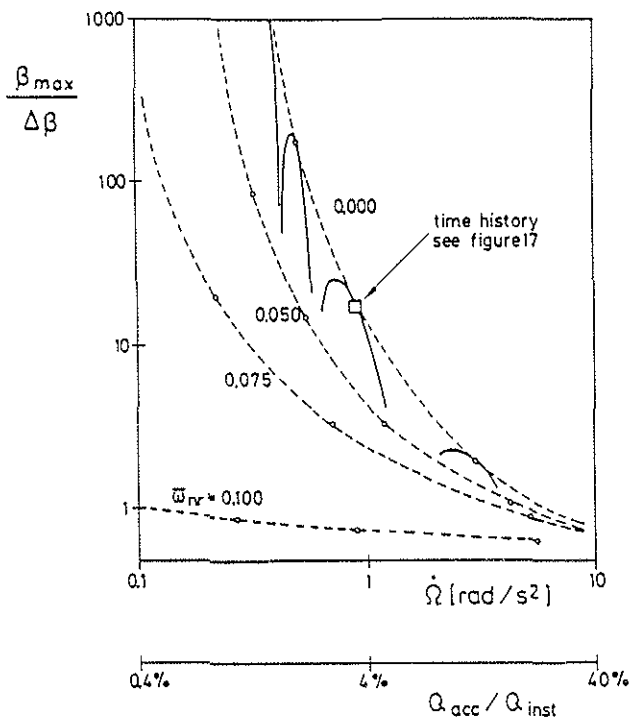


Figure 19: Maximum flapping angle during rotor acceleration procedure with $\Delta\beta$ as excitation of the homogeneous equation

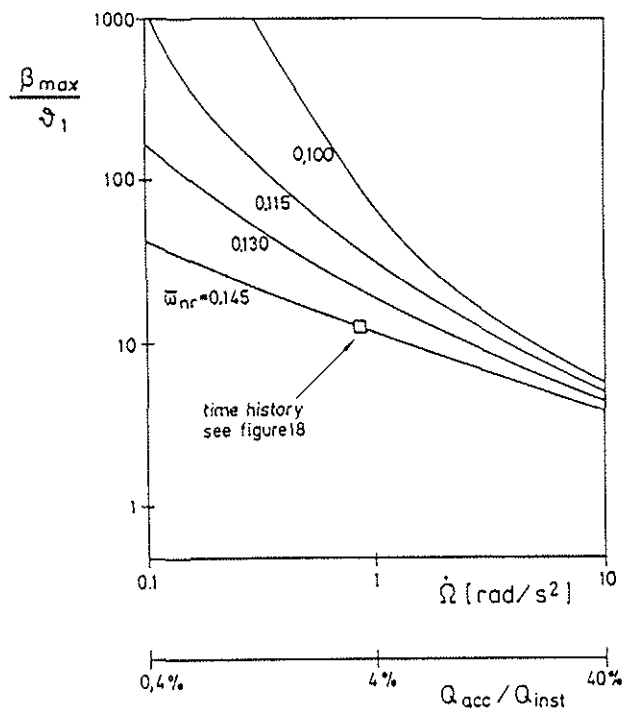


Figure 20: Maximum flapping angle during rotor acceleration procedure with ϑ_1 -term as forcing function of the inhomogeneous equation